
Enabling certification of verification-agnostic networks via memory-efficient semidefinite programming

Sumanth Dathathri^{*1}, Krishnamurthy (Dj) Dvijotham^{*1}, Alex Kurakin^{*2},
Aditi Raghunathan^{*3}, Jonathan Uesato^{*1}, Rudy Bunel¹, Shreya Shankar³,
Jacob Steinhardt⁴, Ian Goodfellow⁵, Percy Liang³, Pushmeet Kohli¹

¹DeepMind ²Google Brain ³Stanford ⁴UC Berkeley ⁵Work done at Google

{dathathri,dvij,kurakin,juesato}@google.com, aditir@stanford.edu

Abstract

Convex relaxations have emerged as a promising approach for verifying desirable properties of neural networks like robustness to adversarial perturbations. Widely used Linear Programming (LP) relaxations only work well when networks are trained to facilitate verification. This precludes applications that involve *verification-agnostic* networks, i.e., networks not specially trained for verification. On the other hand, semidefinite programming (SDP) relaxations have successfully be applied to verification-agnostic networks, but do not currently scale beyond small networks due to poor time and space asymptotics. In this work, we propose a first-order dual SDP algorithm that (1) requires memory only linear in the total number of network activations, (2) only requires a fixed number of forward/backward passes through the network per iteration. By exploiting iterative eigenvector methods, we express all solver operations in terms of forward and backward passes through the network, enabling efficient use of hardware like GPUs/TPUs. For two verification-agnostic networks on MNIST and CIFAR-10, we significantly improve ℓ_∞ verified robust accuracy from 1% \rightarrow 88% and 6% \rightarrow 40% respectively. We also demonstrate tight verification of a quadratic stability specification for the decoder of a variational autoencoder.

1 Introduction

Applications of neural networks to safety-critical domains requires ensuring that they behave as expected under all circumstances [32]. One way to achieve this is to ensure that neural networks conform with a list of *specifications*, i.e., relationships between the inputs and outputs of a neural network that ought to be satisfied. Specifications can come from safety constraints (a robot should never enter certain unsafe states [40, 29, 12]), prior knowledge (a learned physical dynamics model should be consistent with the laws of physics [49]), or stability considerations (certain transformations of the network inputs should not significantly change its outputs [57, 7]).

Evaluating whether a network satisfies a given specification is a challenging task, due to the difficulty of searching for violations over the high dimensional input spaces. Due to this, several techniques that claimed to enhance neural network robustness were later shown to break under stronger attacks [61, 5]. This has motivated the search for verification algorithms that can provide provable guarantees on neural networks satisfying input-output specifications.

Popular approaches based on linear programming (LP) relaxations of neural networks are computationally efficient and have enabled successful verification for many specifications [37, 18, 30, 21]. LP relaxations are sound (they would never incorrectly conclude that a specification is satisfied) but

^{*} Equal contribution. Alphabetical order.

[†] Code available at https://github.com/deepmind/jax_verify.

incomplete (they may fail to verify a specification even if it is actually satisfied). Consequently, these approaches tend to give poor or vacuous results when used in isolation, though can achieve strong results when combined with specific training approaches to aid verification [22, 51, 67, 21, 54, 6].

In contrast, we focus on *verification-agnostic* models, which are trained in a manner agnostic to the verification algorithm. This would enable applying verification to all neural networks, and not just those trained to be verifiable. First, this means training procedures need not be constrained by the need to verify, thus allowing techniques which produce empirically robust networks, which may not be easily verified [38]. Second, ML training algorithms are often not easily modifiable, e.g. production-scale ML models with highly specific pipelines. Third, for many tasks, defining formal specifications is difficult, thus motivating the need to learn specifications from data. In particular, in recent work [24, 50, 66], natural perturbations to images like changes in lighting conditions or changes in the skin tone of a person, have been modeled using perturbations in the latent space of a generative model. In these cases, the specification itself is a verification-agnostic network which the verification must handle even if the prediction network is trained with the verification in mind.

In contrast to LP-based approaches, the semidefinite programming (SDP) relaxation [52] has enabled robustness certification of verification-agnostic networks. However, the interior point methods commonly used for SDP solving are computationally expensive with $O(n^6)$ runtime and $O(n^4)$ memory requirements, where n is the number of neurons in the network [41, 60]. This limits applicability of SDPs to small fully connected neural networks.

Within the SDP literature, a natural approach is to turn to first-order methods, exchanging precision for scalability [63, 53]. Because verification only needs a bound on the optimal value of the relaxation (and not the optimal solution), we need not design a general-purpose SDP solver, and can instead operate directly in the dual. A key benefit is that the dual problem can be cast as minimizing the maximum eigenvalue of an affine function, subject only to non-negativity constraints. This is a standard technique used in the SDP literature [25, 42] and removes the need for an expensive projection operation onto the positive semidefinite cone. Further, since any set of feasible dual variables provides a valid upper bound, we do not need to solve the SDP to optimality as done previously [52], and can instead stop once a sufficiently tight upper bound is attained.

In this paper, we show that applying these ideas to neural network verification results in an efficient implementation both in theory and practice. Our solver requires $O(n)$ memory rather than $O(n^4)$ for interior point methods, and each iteration involves a constant number of forward and backward passes through the network.

Our contributions. The key contributions of our paper are as follows:

1. By adapting ideas from the first-order SDP literature [25, 42], we observe that the dual of the SDP formulation for neural network verification can be expressed as a maximum eigenvalue problem with only interval bound constraints. This formulation generalizes [52] without loss of tightness, and applies to any quadratically-constrained quadratic program (QCQP), including the standard adversarial robustness specification and a variety of network architectures.
Crucially, when applied to neural networks, we show that subgradient computations are expressible purely in terms of forward or backward passes through layers of the neural network. Consequently, applying a subgradient algorithm to this formulation achieves per-iteration complexity comparable to a constant number of forward and backward passes through the neural network.
2. We demonstrate the applicability of first-order SDP techniques to neural network verification. We first evaluate our solver by verifying ℓ_∞ robustness of a variety of *verification-agnostic* networks on MNIST and CIFAR-10. We show that our approach can verify large networks beyond the scope of existing techniques. For these verification-agnostic networks, we obtain bounds an order of magnitude tighter than previous approaches (Figure 1). For an adversarially trained convolutional neural network (CNN) with no additional regularization on MNIST ($\epsilon = 0.1$), compared to LP relaxations, we improve the verified robust accuracy from 1% to 88%. For the same training and architecture on CIFAR-10 ($\epsilon = 2/255$), the corresponding improvement is from 6% to 40% (Table 1).
3. To demonstrate the generality of our approach, we verify a different quadratic specification on the stability of the output of the decoder for a variational autoencoder (VAE). The upper bound on specification violation computed by our solver closely matches the lower bound on specification violation (from PGD attacks) across a wide range of inputs (Section 6.2).

2 Related work

Neural network verification. There is a large literature on verification methods for neural networks. Broadly, the literature can be grouped into complete verification using mixed-integer programming [26, 18, 59, 10, 2], bound propagation [56, 70, 65, 21], convex relaxation [30, 17, 67, 51], and randomized smoothing [35, 11]. Verified training approaches when combined with convex relaxations have led to promising results [30, 51, 23, 6]. Randomized smoothing and verified training approaches requires special modifications to the predictor (smoothing the predictions by adding noise) and/or the training algorithm (training with additional noise or regularizers) and hence are not applicable to the verification-agnostic setting. Bound propagation approaches have been shown to be special instances of LP relaxations [37]. Hence we focus on describing the convex relaxations and complete solvers, as the areas most closely related to this paper.

Complete verification approaches. These methods rely on exhaustive search to find counter-examples to the specification, using smart propagation or bounding methods to rule out parts of the search space that are determined to be free of counter-examples. The dominant paradigms in this space are Satisfiability Modulo Theory (SMT) [26, 18] and Mixed Integer Programming (MIP) [59, 10, 2]. The two main issues with these solvers are that: 1) They can take exponential time in the network size and 2) They typically cannot run on accelerators for deep learning (GPUs, TPUs).

Convex relaxation based methods. Much work has relied on linear programming (LP) or similar relaxations for neural-network verification [30, 17]. Bound propagation approaches can also be viewed as a special case of LP relaxations [37]. Recent work [54] put all these approaches on a uniform footing and demonstrated using extensive experiments that there are fundamental barriers in the tightness of these LP based relaxations and that obtaining tight verification procedures requires better relaxations. A similar argument in [52] demonstrated a large gap between LP and SDP relaxations even for networks with randomly chosen weights. Fazlyab et al. [19, 20] generalized the SDP relaxations to arbitrary network structures and activation functions. However, these papers use off-the-shelf interior point solvers to solve the resulting relaxations, preventing them from scaling to large CNNs. In this paper, we focus on SDP relaxations but develop customized solvers that can run on accelerators for deep learning (GPUs/TPUs) enabling their application to large CNNs.

First-order SDP solvers. While interior-point methods are theoretically compelling, the demands of large-scale SDPs motivate first-order solvers. Common themes within this literature include smoothing of nonsmooth objectives [42, 33, 14] and spectral bundle or proximal methods [25, 36, 45]. Conditional gradient methods use a sum of rank-one updates, and when combined with sketching techniques, can represent the primal solution variable using linear space [68, 69]. Many primal-dual algorithms [64, 63, 41, 4, 15] exploit computational advantages of operating in the dual – in fact, our approach to verification operates exclusively in the dual, thus sidestepping space and computational challenges associated with the primal matrix variable. Our formulation in Section 5.1 closely follows the eigenvalue optimization formulation from Section 3 of Helmborg and Rendl [25]. While in this work, we show that vanilla subgradient methods are sufficient to achieve practical performance for many problems, many ideas from the first-order SDP literature are promising candidates for future work, and could potentially allow faster or more reliable convergence. A full survey is beyond scope here, but we refer interested readers to Tu and Wang [60] and the related work of Yurtsever et al. [69] for excellent surveys.

3 Verification setup

Notation. For vectors a, b , we use $a \leq b$ and $a \geq b$ to represent element-wise inequalities. We use $\mathcal{B}_\epsilon(x)$ to denote the ℓ_∞ ball of size ϵ around input x . For symmetric matrices X, Y , we use $X \geq Y$ to denote that $X - Y$ is positive semidefinite (i.e. $X - Y$ is a symmetric matrix with non-negative eigenvalues) We use $[x]^+$ to denote $\max(x, 0)$ and $[x]^-$ for $\min(x, 0)$. $\mathbf{1}$ represents a vector of all ones.

Neural networks. We are interested in verifying properties of neural network with L hidden layers and N neurons that takes input x_0 . x_i denotes the activations at layer i and the concatenated vector $x = [x_0, x_1, x_2, \dots, x_L]$ represents all the activations of the network. Let \mathbb{L}_i denote an affine map corresponding to a forward pass through layer i , for e.g., linear, convolutional and average pooling layers. Let σ_i is an element-wise activation function, for e.g., ReLU, sigmoid, tanh. In this work, we focus on feedforward networks where $x_{i+1} = \sigma_i(\mathbb{L}_i(x_i))$.

Verification. We study verification problems that involve determining whether $\phi(x) \leq 0$ for network inputs x_0 satisfying $\ell_0 \leq x_0 \leq u_0$ where specification ϕ is a function of the network activations x .

$$\text{opt} =: \max_x \phi(x) \quad \text{subject to} \quad \underbrace{x_{i+1} = \sigma_i(\mathbb{L}_i(x_i))}_{\text{Neural net constraints}}, \underbrace{\ell_0 \leq x_0 \leq u_0}_{\text{Input constraints}}. \quad (1)$$

The property is verified if $\text{opt} \leq 0$. In this work, we focus on ϕ which are quadratic functions. This includes several interesting properties like verification of adversarial robustness (where ϕ is linear), conservation of an energy in dynamical systems [49], or stability of VAE decoders (Section 6.2). Note that while we assume ℓ_∞ -norm input constraints for ease of presentation, our approach is applicable to any quadratic input constraint.

4 Lagrangian relaxation of QCQPs for verification

A starting point for our approach is the following observation from prior work—the neural network constraints in the verification problem (1) can be replaced with quadratic constraints for ReLUs [52] and other common activations [19], yielding a Quadratically Constrained Quadratic Program (QCQP). We bound the solution to the resulting QCQP via a Lagrangian relaxation. Following [52], we assume access to lower and upper bounds ℓ_i, u_i on activations x_i such that $\ell_i \leq x_i \leq u_i$. They can be obtained via existing bound propagation techniques [65, 30, 70]. We use $\ell \leq x \leq u$ to denote the collection of activations and bounds at all the layers taken together.

We first describe the terms in the Lagrangian corresponding to the constraints encoding layer i in a ReLU network: $x_{i+1} = \text{ReLU}(\mathbb{L}_i(x_i))$. Let ℓ_i, u_i denote the bounds such that $\ell_i \leq x_i \leq u_i$. We associate Lagrange multipliers $\lambda_i = [\lambda_i^a; \lambda_i^b; \lambda_i^c; \lambda_i^d]$ corresponding to each of the constraints as follows.

$$\begin{aligned} x_{i+1} &\geq 0 \quad [\lambda_i^a], \quad x_{i+1} \geq \mathbb{L}_i(x_i) \quad [\lambda_i^b] \\ x_{i+1} \odot (x_{i+1} - \mathbb{L}_i(x_i)) &\leq 0 \quad [\lambda_i^c], \quad x_i \odot x_i - (\ell_i + u_i) \odot x_i + \ell_i \odot u_i \leq 0 \quad [\lambda_i^d]. \end{aligned} \quad (2)$$

The linear constraints imply that x_{i+1} is greater than both 0 and $\mathbb{L}_i(x_i)$. The first quadratic constraint together with the linear constraint makes x_{i+1} equal to the larger of the two, i.e. $x_{i+1} = \max(\mathbb{L}_i(x_i), 0)$. The second quadratic constraint directly follows from the bounds on the activations. The Lagrangian $\mathcal{L}(x_i, x_{i+1}, \lambda_i)$ corresponding to the constraints and Lagrange multipliers described above is as follows.

$$\begin{aligned} \mathcal{L}(x_i, x_{i+1}, \lambda_i) &= (-x_{i+1})^\top \lambda_i^a + (\mathbb{L}_i(x_i) - x_{i+1})^\top \lambda_i^b \\ &\quad + (x_{i+1} \odot (x_{i+1} - \mathbb{L}_i(x_i)))^\top \lambda_i^c + (x_i \odot x_i - (\ell_i + u_i) \odot x_i + \ell_i \odot u_i)^\top \lambda_i^d \\ &= \underbrace{(\ell_i \odot u_i)^\top \lambda_i^d}_{\text{independent of } x_i, x_{i+1}} - \underbrace{x_{i+1}^\top \lambda_i^a + (\mathbb{L}_i(x_i))^\top \lambda_i^b - x_{i+1}^\top \lambda_i^c - x_i^\top ((\ell_i + u_i) \odot \lambda_i^d)}_{\text{linear in } x_i, x_{i+1}} \\ &\quad + \underbrace{x_{i+1}^\top \text{diag}(\lambda_i^c) x_{i+1} - x_{i+1}^\top \text{diag}(\lambda_i^c) \mathbb{L}_i(x_i) + x_i^\top \text{diag}(\lambda_i^d) x_i}_{\text{Quadratic in } x_i, x_{i+1}}. \end{aligned} \quad (3)$$

The overall Lagrangian $\mathcal{L}(x, \lambda)$ is the sum of $\mathcal{L}(x_i, x_{i+1}, \lambda_i)$ across all layers together with the objective $\phi(x)$, and consists of terms that are either independent of x , linear in x or quadratic in x . Thus, $\mathcal{L}(x, \lambda)$ is a quadratic polynomial in x and can be written in the form $\mathcal{L}(x, \lambda) = c(\lambda) + x^\top g(\lambda) + \frac{1}{2} x^\top H(\lambda) x$. Each of the coefficients $c(\lambda)$, $g(\lambda)$, and $H(\lambda)$ are affine as a function of λ . We will describe our approach in terms of $c(\lambda)$, $g(\lambda)$, and $H(\lambda)$, which need not be derived by hand, and can instead be directly obtained from the Lagrangian $\mathcal{L}(x, \lambda)$ via automatic differentiation as we discuss in Section 5.2. We observe that $\mathcal{L}(x, \lambda)$ is itself composed entirely of forward passes $\mathbb{L}_i(x_i)$ and element-wise operations. This makes computing $\mathcal{L}(x, \lambda)$ both convenient to implement and efficient to compute in deep learning frameworks.

Via standard Lagrangian duality, the Lagrangian provides a bound on opt :

$$\text{opt} \leq \min_{\lambda \geq 0} \max_{\ell \leq x \leq u} \mathcal{L}(x, \lambda) = \min_{\lambda \geq 0} \max_{\ell \leq x \leq u} c(\lambda) + x^\top g(\lambda) + \frac{1}{2} x^\top H(\lambda) x. \quad (4)$$

We now describe our dual problem formulation starting from this Lagrangian (4).

5 Scalable and Efficient SDP-relaxation Solver

Our goal is to develop a custom solver for large-scale neural network verification with the following desiderata: (1) compute *anytime* upper bounds valid after each iteration, (2) rely on elementary

computations with efficient implementations that can exploit hardware like GPUs and TPUs, and (3) have per-iteration memory and computational cost that scales linearly in the number of neurons.

In order to satisfy these desiderata, we employ first order methods to solve the Lagrange dual problem (4). We derive a reformulation of the Lagrange dual with only non-negativity constraints on the decision variables (Section 5.1). We then show how to efficiently and conveniently compute subgradients of the objective function in Section 5.2 and derive our final solver in Algorithm 1.

5.1 Reformulation to a problem with only non-negativity constraints

Several algorithms in the first-order SDP literature rely on reformulating the semidefinite programming problem as an eigenvalue minimization problem [25, 42]. Applying this idea, we obtain a Lagrange dual problem which only has non-negativity constraints and whose subgradients can be computed efficiently, enabling efficient projected subgradient methods to be applied.

Recall that ℓ_i, u_i denote precomputed lower and upper bounds on activations x_i . For simplicity in presentation, we assume $\ell_i = -1$ and $u_i = 1$ respectively for all i . This is without loss of generality, since we can always center and rescale the activations based on precomputed bounds to obtain normalized activations $\bar{x} \in [-1, 1]$ and express the Lagrangian in terms of the normalized activations \bar{x} .

Proposition 1. The optimal value opt of the verification problem (1) is bounded above by the Lagrange dual problem corresponding to the Lagrangian in (4) which can be written as follows:

$$\text{opt}_{\text{relax}} =: \min_{\lambda \geq 0, \kappa \geq 0} \underbrace{c(\lambda) + \frac{1}{2} \mathbf{1}^\top \left[\kappa - \lambda_{\min}^- (\text{diag}(\kappa) - M(\lambda)) \mathbf{1} \right]}_{f(\lambda, \kappa)}, \quad M(\lambda) = \begin{pmatrix} 0 & g(\lambda)^\top \\ g(\lambda) & H(\lambda) \end{pmatrix}, \quad (5)$$

and $\lambda_{\min}^-(Z) = \min(\lambda_{\min}(Z), 0)$ is the negative portion of the smallest eigenvalue of Z and $\kappa \in \mathbb{R}^{1+N}$.

Proof Sketch. Instead of directly optimizing over the primal variables x in the Lagrangian of the verification problem (4), we explicitly add the redundant constraint $x^2 \leq 1$ with associated dual variables κ , and then optimize over x in closed form. This does not change the the primal (or dual) optimum, but makes the constraints in the dual problem simpler. In the corresponding Lagrange dual problem (now over λ, κ), there is a PSD constraint of the form $\text{diag}(\kappa) \geq M(\lambda)$. Projecting onto this constraint directly is expensive and difficult. However, for any $(\lambda, \kappa) \geq 0$, we can construct a dual feasible solution $(\lambda, \hat{\kappa})$ by simply subtracting the smallest eigenvalue of $\text{diag}(\kappa) - M(\lambda)$, if negative. For any non-negative λ, κ , the final objective $f(\lambda, \kappa)$ is the objective of the corresponding dual feasible solution and the bound follows from standard Lagrangian duality. The full proof appears in Appendix A.3. \square

Remark 1. Raghunathan et al. [52] present an SDP relaxation to the QCQP for the verification of ℓ_∞ adversarial robustness. The solution to their SDP is equal to $\text{opt}_{\text{relax}}$ in our formulation (5) (Appendix A.4). Raghunathan et al. [52] solve the SDP via interior-point methods using off-the-shelf solvers which simply cannot scale to larger networks due to memory requirement that is quartic in the number of activations. In contrast, our algorithm (Algorithm 1) has memory requirements that scale linearly in the number of activations.

Remark 2. Our proof is similar to the standard maximum eigenvalue transformation for the SDP dual, as used in Helmberg and Rendl [25] or Nesterov [42] (see Appendix A.6 for details). Crucially for scalable implementation, our formulation avoids explicitly computing or storing the matrices for either the primal or dual SDPs. Instead, we will rely on automatic differentiation of the Lagrangian and matrix-vector products to represent these matrices implicitly, and achieve linear memory and runtime requirements. We discuss this approach now.

5.2 Efficient computation of subgradients

Our formulation in (5) is amenable to first-order methods. Projections onto the feasible set are simple and we now show how to efficiently compute the subgradient of the objective $f(\lambda, \kappa)$. By Danskin’s theorem [13],

$$\partial_{\lambda, \kappa} \left(c(\lambda) + \frac{1}{2} \mathbf{1}^\top \left[\kappa - [v^{*\top} (\text{diag}(\kappa) - M(\lambda)) v^*] \mathbf{1} \right] \right) \in \partial_{\lambda, \kappa} f(\lambda, \kappa), \quad (6a)$$

$$\text{where } v^* = \underset{\|v\|=1}{\text{argmin}} v^\top (\text{diag}(\kappa) - M(\lambda)) v = \text{eigmin}(\text{diag}(\kappa) - M(\lambda)), \quad (6b)$$

and $\partial_{\lambda,\kappa}$ denotes the subdifferential with respect to λ,κ . In other words, given any eigenvector v^* corresponding to the minimum eigenvalue of the matrix $\text{diag}(\kappa) - M(\lambda)$, we can obtain a valid subgradient by applying autodiff to the left-hand side of (6a) while treating v^* as fixed.¹ The main computational difficulty is computing v^* . While our final certificate will use an exact eigendecomposition for v^* , for our subgradient steps, we can approximate v^* using an iterative method such as Lanczos [34]. Lanczos only requires repeated applications of the linear map $\mathbb{A} =: v \mapsto (\text{diag}(\kappa) - M(\lambda))v$. This linear map can be easily represented via derivatives and Hessian-vector products of the Lagrangian.

Implementing implicit matrix-vector products via autodiff. Recall from Section 4 that the Lagrangian is expressible via forward passes through affine layers and element-wise operations involving adjacent network layers. Since $M(\lambda)$ is composed of the gradient and Hessian of the Lagrangian, we will show computing the map $M(\lambda)v$ is computationally roughly equal to a forwards+backwards pass through the network. Furthermore, implementing this map is extremely convenient in ML frameworks supporting autodiff like TensorFlow [1], PyTorch [47], or JAX [8]. From the Lagrangian (4), we note that

$$g(\lambda) = \mathcal{L}_x(0,\lambda) = \left. \frac{\partial \mathcal{L}(x,\lambda)}{\partial x} \right|_{0,\lambda} \quad \text{and} \quad H(\lambda)v = \mathcal{L}_{xx}^v(0,\lambda,v) = \left. \left(\frac{\partial^2 \mathcal{L}(x,\lambda)}{\partial x \partial x^T} \right) \right|_{0,\lambda} v = \left. \frac{\partial v^\top \mathcal{L}_x(0,\lambda)}{\partial x} \right|_{0,\lambda}.$$

Thus, $g(\lambda)$ involves a single gradient, and by using a standard trick for Hessian-vector products [48], the Hessian-vector product $H(\lambda)v$ requires roughly double the cost of a standard forward-backwards pass, with linear memory overhead. From the definition of $M(\lambda)$ in (5), we can use the quantities above to get

$$\mathbb{A}[v] = (\text{diag}(\kappa) - M(\lambda))v = -\kappa \odot v + \begin{pmatrix} (g(\lambda))^\top v_{1:N} \\ g(\lambda)v_0 + H(\lambda)v_{1:N} \end{pmatrix} = \kappa \odot v - \begin{pmatrix} (\mathcal{L}_x(0,\lambda))^\top v_{1:N} \\ \mathcal{L}_x(0,\lambda)v_0 + \mathcal{L}_{xx}^v(0,\lambda,v_{1:N}) \end{pmatrix},$$

where v_0 is the first coordinate of v and $v_{1:N}$ is the subvector of v formed by remaining coordinates.

5.3 Practical tricks for faster convergence

The Lagrange dual problem is a convex optimization problem, and a projected subgradient method with appropriately decaying step-sizes converges to an optimal solution [43]. However, we can achieve faster convergence in practice through careful choices for initialization, regularization, and learning rates.

Initialization. Let $\kappa_{\text{opt}}(\lambda)$ denote the value of κ that optimizes the bound (5), for a fixed λ . We initialize with $\lambda = 0$, and the corresponding $\kappa_{\text{opt}}(0)$ using the following proposition.

Proposition 2. For any choice of λ satisfying $H(\lambda) = 0$, the optimal choice $\kappa_{\text{opt}}(\lambda)$ is given by

$$\kappa_0^* = \sum_{i=1}^n |g(\lambda)|_i \quad ; \quad \kappa_{1:n}^* = |g(\lambda)|$$

where $\kappa = [\kappa_0; \kappa_{1:n}]$ is divided into a leading scalar κ_0 and vector $\kappa_{1:n}$, and $|g(\lambda)|$ is elementwise.

See Appendix A.7 for a proof. Note that when $\phi(x)$ is linear, $H(\lambda) = 0$ is equivalent to removing the quadratic constraints on the activations and retaining the linear constraints in the Lagrangian (4).

Regularization. Next, we note that there always exists an optimal dual solution satisfying $\kappa_{1:n} = 0$, because they are the Lagrange multipliers of a redundant constraint; full proof appears in Appendix A.5. However, κ has an empirical benefit of smoothing the optimization by preventing negative eigenvalues of \mathbb{A} . This is mostly noticeable in the early optimization steps. Thus, we can regularize κ through either an additional loss term $\sum \kappa_{1:n}$, or by fixing $\kappa_{1:n}$ to zero midway through optimization. In practice, we found that both options occasionally improve final performance.

Learning rates. Empirically, we observed that the optimization landscape varies significantly for dual variables associated with different constraints (such as linear vs. quadratic). In practice, we found that using adaptive optimizers [16] such as Adam [27] or RMSProp [58] was necessary to stabilize optimization. Additional learning rate adjustment for κ_0 and the dual variables corresponding to the quadratic ReLU constraints provided an improvement on some network architectures (see Appendix B).

5.4 Algorithm for verifying network specifications

¹ The subgradient is a singleton except when the multiplicity of the minimum eigenvalue is greater than one, in which case any minimal eigenvector yields a valid subgradient.

Algorithm 1 Verification via SDP-FO

Input: Specification ϕ and bounds on the inputs $\ell_0 \leq x_0 \leq u_0$

Output: Upper bound on the optimal value of (1)

Bound computation: Obtain layer-wise bounds $\ell, u = \text{BoundProp}(\ell_0, u_0)$ using approaches such as [39, 70]

Lagrangian: Define Lagrangian $\mathcal{L}(x, \lambda)$ from (4)

Initialization: Initialize λ, κ (Section 5.3)

for $t = 1, \dots, T$ **do**

Define the linear operator \mathbb{A}_t as $\mathbb{A}_t[v] = \kappa \odot v - \begin{pmatrix} (\mathcal{L}_x(0, \lambda))^\top v_1 \\ \mathcal{L}_x(0, \lambda)v_0 + \mathcal{L}_{xx}^v(0, \lambda, v_1) \end{pmatrix}$ (see section 5.2)

$v^* \leftarrow \text{eigmin}(\mathbb{A}_t)$ using the Lanczos algorithm [34].

Define the function $f_t(\lambda, \kappa) = \mathcal{L}(0, \lambda) + \left[\kappa - [v^{*\top} \mathbb{A}_t[v^*]] \mathbf{1} \right]^+ \mathbf{1}$ (see (6))

$\bar{f}_t \leftarrow f_t(\lambda^t, \kappa^t)$

Update λ^t, κ^t using any gradient based method to obtain $\tilde{\lambda}, \tilde{\kappa}$ with the gradients: $\frac{\partial}{\partial \lambda} f_t(\lambda^t, \kappa^t), \frac{\partial}{\partial \kappa} f_t(\lambda^t, \kappa^t)$

Project $\lambda^{t+1} \leftarrow [\tilde{\lambda}]^+, \kappa^{t+1} \leftarrow [\tilde{\kappa}]^+$.

end for

return $\min_t \bar{f}_t$

We refer to our algorithm (summarized in Algorithm 1) as SDP-FO since it relies on a first-order method to solve the SDP relaxation. Although the full algorithm involves several components, the implementation is simple (~100 lines for the core logic when implemented in JAX[9]) and easily applicable to general architectures and specifications.² SDP-FO uses memory linear in the total number of network activations, with per-iteration runtime linear in the cost of a forwards-backwards pass.

Computing valid certificates. Because Lanczos is an approximate method, we always report final bounds by computing v^* using a non-iterative exact eigen-decomposition method from SciPy [44]. In practice, the estimates from Lanczos are very close to the exact values, while using 0.2s/iteration on large convolutional network, compared to 5 minutes for exact eigendecomposition (see Appendix C).

6 Experiments

In this section, we evaluate our SDP-FO verification algorithm on two specifications: robustness to adversarial perturbations for image classifiers (Sec. 6.1), and robustness to latent space perturbations for a generative model (Sec. 6.2). In both cases, we focus on verification-agnostic networks.

6.1 Verification of adversarial robustness

Metrics and baselines We first study verification of ℓ_∞ robustness for networks trained on MNIST and CIFAR-10. For this specification, the objective $\phi(x)$ in (1) is given by $(x_L)_{y'} - (x_L)_y$, where x_L denotes the the final network activations, i.e. logits, y is the index of the true image label, and y' is a target label. For each image and target label, we obtain a lower bound on the optimal $\underline{\phi}(x) \leq \phi^*(x)$ by running projected gradient descent (PGD) [38] on the objective $\phi(x)$ subject to ℓ_∞ input constraints. A verification technique provides upper bounds $\bar{\phi}(x) \geq \phi^*(x)$. An example is said to be verified when the worst-case upper bound across all possible labels, denoted $\bar{\phi}_x$, is below 0. We first compare (SDP-FO, Algorithm 1) to the LP relaxation from [18], as this is a widely used approach for verifying large networks, and is shown by [55] to encompass other relaxations including [30, 17, 65, 70, 39, 23]. We further compare to the SDP relaxation from [51] solved using MOSEK [3], a commercial interior point SDP (SDP-IP) solver, and the MIP approach from [59].

Models Our main experiments on CNNs use two architectures: CNN-A from [67] and CNN-B from [6]. These contain roughly 200K parameters + 10K activations, and 2M parameters + 20K activations, respectively. All the networks we study are verification-agnostic: trained only with nominal and/or adversarial training [38], without any regularization to promote verifiability.

While these networks are much smaller than modern deep neural networks, they are an order of magnitude larger than previously possible for verification-agnostic networks. To compare with prior

² Core solver implementation at https://github.com/deepmind/jax_verify/blob/master/src/sdp_verify/sdp_verify.py

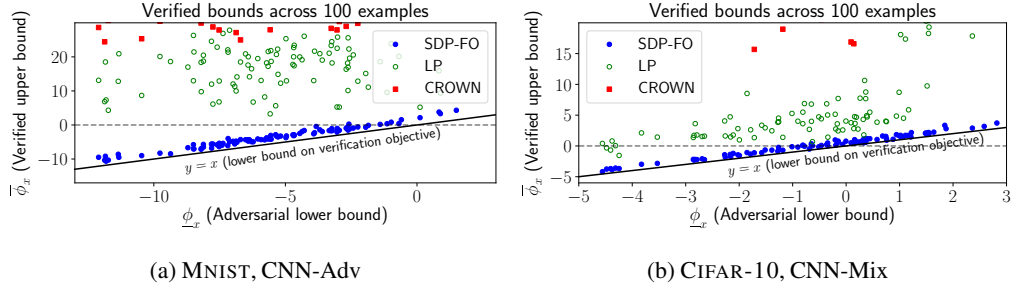


Figure 1: *Enabling certification of verification-agnostic networks.* For 100 random examples on MNIST and CIFAR-10, we plot the verified upper bound on ϕ_x against the adversarial lower bound (taking the worst-case over target labels for each). Recall, an example is verified when the verified upper bound $\bar{\phi}_x < 0$. Our key result is that SDP-FO achieves tight verification across all examples, with all points lying close to the line $y = x$. In contrast, LP or CROWN bounds produce much looser gaps between the lower and upper bounds. We note that many CROWN bounds exceed the plotted y-axis limits.

work, we also evaluate a variety of fully-connected **MLP** networks, using trained parameters from [51, 55]. These each contain roughly 1K activations. Complete training and hyperparameter details are included in Appendix B.1.

Scalable verification of verification-agnostic networks Our central result is that, for verification-agnostic networks, SDP-FO allows us to tractably provide significantly stronger robustness guarantees in comparison with existing approaches. In Figure 1, we show that SDP-FO reliably achieves tight verification, despite using loose initial lower and upper bounds obtained from CROWN [70] in Algorithm 1. Table 1 summarizes results. On all networks we study, we significantly improve on the baseline verified accuracies. For example, we improve verified robustness accuracy for CNN-A-Adv on MNIST from 0.4% to 87.8% and for CNN-A-Mix on CIFAR-10 from 5.8% to 39.6%.

Dataset	Epsilon	Model	Accuracy		Verified Accuracy			
			Nominal	PGD	SDP-FO (Ours)	SDP-IP [†]	LP	MIP [‡]
MNIST	$\epsilon = 0.1$	MLP-SDP [52]	97.6%	86.4%	85.2%	80%	39.5%	69.2%
		MLP-LP [52]	92.8%	81.2%	80.2%	80%	79.4%	-
		MLP-Adv [52]	98.4%	93.4%	91.0%	82%	26.6%	-
		MLP-Adv-B [55]	96.8%	84.0%	79.2%	-	33.2%	34.4%
		CNN-A-Adv	99.1%	95.2%	87.8%	-	0.4%	-
	$\epsilon = 0.05$	MLP-Nor [55]	98.0%	46.6%	28.0%	-	1.8%	6.0%
CIFAR-10	$\epsilon = \frac{2}{255}$	CNN-A-Mix-4	67.8%	55.6%	47.8%	*	26.8%	-
		CNN-B-Adv-4	72.0%	62.0%	46.0%	*	20.4%	-
		CNN-A-Mix	74.2%	53.0%	39.6%	*	5.8%	-
		CNN-B-Adv	80.3%	64.0%	32.8%	*	2.2%	-

[†] Using numbers from [52] for SDP-IP and [54] using approach of [59] for MIP. Dashes indicate previously reported numbers are unavailable.
^{*} Computationally infeasible due to quartic memory requirement.

Table 1: Comparison of verified accuracy across verification algorithms. Highlighted rows indicate models trained in a verification-agnostic manner. All numbers computed across the same 500 test set examples, except when using previously reported values. For all networks, SDP-FO outperforms previous approaches. The improvement is largest for verification-agnostic models.

Comparisons on small-scale problems We empirically compare SDP-FO against SDP-IP using MOSEK, a commercial interior-point solver. Since the two formulations are equivalent (see Appendix A.4), solving them to optimality should result in the same objective. This lets us carefully isolate the effectiveness of the optimization procedure relative to the SDP relaxation gap. However, we note that for interior-point methods, the memory requirements are quadratic in the size of $M(\lambda)$, which becomes quickly intractable e.g. ≈ 10 petabytes for a network with 10K activations. This restricts our comparison to the small MLP networks from [52], while SDP-FO can scale to significantly larger networks.

In Figure 4 of Appendix C.1, we confirm that on a small random subset of matching verification instances, SDP-FO bounds are only slightly worse than SDP-IP bounds. This suggests that optimization is typically not an issue for SDP-FO, and the main challenge is instead tightening the SDP relaxation. Indeed, we can tighten the relaxation by using CROWN precomputed bounds [70] rather than interval

arithmetic bounds [39, 22], which almost entirely closes the gap between SDP-FO and PGD for the first three rows of Table 1, including the verification-agnostic MLP-Adv. Finally, compared to numbers reported in [55], SDP-FO outperforms the MIP approach using progressive LP bound tightening [59].

Computational resources We cap the number of projected gradient iterations for SDP-FO. Using a P100 GPU, maximum runtime is roughly 15 minutes per MLP instances, and 3 hours per CNN instances, though most instances are verified sooner. For reference, SDP-IP uses 25 minutes on a 4-core CPU per MLP instance [52], and is intractable for CNN instances due to quartic memory usage.

Limitations. In principle, our solver’s linear asymptotics allow scaling to extremely large networks. However, in practice, we observe loose bounds with large networks. In Table 1, there is already a significantly larger gap between the PGD and SDP-FO bounds for the larger CNN-B models compared to their CNN-A counterparts, and in preliminary experiments, this gap increases further with network size. Thus, while our results demonstrate that the SDP relaxation remains tight on significantly larger networks than those studied in Raghunathan et al. [52], additional innovations in either the formulation or optimization process are necessary to enable further scaling.

6.2 Verifying variational auto-encoders (VAEs)

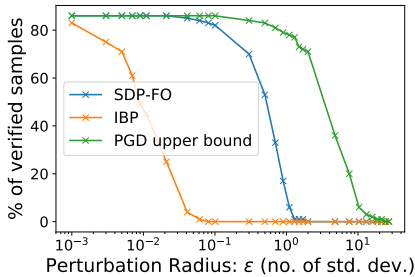


Figure 2: Comparison of different approaches for verifying the robustness of the decoder of a VAE on MNIST, measured across 100 samples. The lower-bound on the robust accuracy computed with SDP-FO closely matches the upper bound based on a PGD adversarial attack upto perturbations of $0.1 \sigma_z$, while the lower bound based on IBP begins to diverge from the PGD upper bound at much smaller perturbations.

Setup To test the generality of our approach, we consider a different specification of verifying the validity of constructions from deep generative models, specifically variational auto-encoders (VAEs) [28]. Let $q_E(z|s) = \mathcal{N}(\mu_E^{z;s}, \sigma_E^{z;s})$ denote the distribution of the latent representation z corresponding to input s , and let $q_D(s|z) = \mathcal{N}(\mu_D^{s;z}, I)$ denote the decoder. Our aim is to certify robustness of the decoder to perturbations in the VAE latent space. Formally, the VAE decoder is robust to ℓ_∞ latent perturbations for input s and perturbation radius $\alpha \in \mathbb{R}^{++}$ if:

$$\varepsilon_{\text{recon}}(s, \mu_D^{s;z}) := \|s - \mu_D^{s;z}\|_2^2 \leq \tau \quad \forall z' \text{ s.t. } \|z' - \mu_E^{z;s}\|_\infty \leq \alpha \sigma_E^{z;s}, \quad (7)$$

where $\varepsilon_{\text{recon}}$ is the reconstruction error. Note that unlike the adversarial robustness setting where the objective was linear, the objective function $\varepsilon_{\text{recon}}$ is quadratic. Quadratic objectives are not directly amenable to LP or MIP solvers without further relaxing the quadratic objective to a linear one. For varying perturbation radii α , we measure the test set fraction with verified reconstruction error below $\tau = 40.97$, which is the median squared Euclidean distance between a point s and the closest point with a different label (over MNIST).

Results We verify a VAE on MNIST with a convolutional decoder containing $\approx 10\text{K}$ total activations. Figure 2 shows the results. To visualize the improvements resulting from our solver, we include a comparison with guarantees based on interval arithmetic bound propagation (IBP) [23, 39], which we use to generate the bounds used in Algorithm 1. Compared to IBP, SDP-FO can successfully verify at perturbation radii roughly 50x as large. For example, IBP successfully verifies 50% at roughly $\epsilon = 0.01$ compared to $\epsilon = 0.5$ for SDP-FO. We note that besides the IBP bounds being themselves loose compared to the SDP relaxations, they further suffer from a similar drawback as LP/MIP methods in that they bound $\varepsilon_{\text{recon}}$ via ℓ_∞ -bounds, which further results in looser bounds on $\varepsilon_{\text{recon}}$. Further details and visualizations are included in Appendix B.2.

7 Conclusion

We have developed a promising approach to scalable tight verification and demonstrated good performance on larger scale than was possible previously. While in principle, this solver is applicable to arbitrarily large networks, further innovations (in either the formulation or solving process) are necessary to get meaningful verified guarantees on larger networks.

Acknowledgements

We are grateful to Yair Carmon, Ollie Hinder, M Pawan Kumar, Christian Tjandraatmadja, Vincent Tjeng, and Rahul Trivedi for helpful discussions and suggestions. This work was supported by NSF Award Grant no. 1805310. AR was supported by a Google PhD Fellowship and Open Philanthropy Project AI Fellowship.

Broader Impact

Our work enables verifying properties of verification-agnostic neural networks trained using procedures agnostic to any specification verification algorithm. While the present scalability of the algorithm does not allow it to be applied to SOTA deep learning models, in many applications it is vital to verify properties of smaller models running safety-critical systems (learned controllers running on embedded systems, for example). The work we have presented here does not address data related issues directly, and would be susceptible to any biases inherent in the data that the model was trained on. However, as a verification technique, it does not enhance biases present in any pre-trained model, and is only used as a post-hoc check. We do not envisage any significant harmful applications of our work, although it may be possible for adversarial actors to use this approach to verify properties of models designed to induce harm (for example, learning based bots designed to break spam filters or induce harmful behavior in a conversational AI system).

References

- [1] Martín Abadi, Paul Barham, Jianmin Chen, Zhifeng Chen, Andy Davis, Jeffrey Dean, Matthieu Devin, Sanjay Ghemawat, Geoffrey Irving, Michael Isard, et al. Tensorflow: A system for large-scale machine learning. In *12th {USENIX} Symposium on Operating Systems Design and Implementation* ({OSDI} 16), pages 265–283, 2016.
- [2] Ross Anderson, Joey Huchette, Will Ma, Christian Tjandraatmadja, and Juan Pablo Vielma. Strong mixed-integer programming formulations for trained neural networks. *Mathematical Programming*, pages 1–37, 2020.
- [3] MOSEK ApS. *The MOSEK optimization toolbox for MATLAB manual. Version 9.0.*, 2019. URL <http://docs.mosek.com/9.0/toolbox/index.html>.
- [4] Sanjeev Arora and Satyen Kale. A combinatorial, primal-dual approach to semidefinite programs. *J. ACM*, 63(2), May 2016. ISSN 0004-5411. doi: 10.1145/2837020. URL <https://doi.org/10.1145/2837020>.
- [5] Anish Athalye, Nicholas Carlini, and David Wagner. Obfuscated gradients give a false sense of security: Circumventing defenses to adversarial examples. *arXiv preprint arXiv:1802.00420*, 2018.
- [6] Mislav Balunovic and Martin Vechev. Adversarial training and provable defenses: Bridging the gap. In *International Conference on Learning Representations*, 2020. URL <https://openreview.net/forum?id=SJxSDxrKDr>.
- [7] Battista Biggio, Iginio Corona, Davide Maiorca, Blaine Nelson, Nedim Šrđić, Pavel Laskov, Giorgio Giacinto, and Fabio Roli. Evasion attacks against machine learning at test time. In *Joint European conference on machine learning and knowledge discovery in databases*, pages 387–402. Springer, 2013.
- [8] James Bradbury, Roy Frostig, Peter Hawkins, Matthew James Johnson, Chris Leary, Dougal Maclaurin, and Skye Wanderman-Milne. Jax: composable transformations of python+ numpy programs, 2018. URL <http://github.com/google/jax>, page 18.
- [9] James Bradbury, Roy Frostig, Peter Hawkins, Matthew James Johnson, Chris Leary, Dougal Maclaurin, and Skye Wanderman-Milne. JAX: composable transformations of Python+NumPy programs, 2018. URL <http://github.com/google/jax>.
- [10] Rudy R Bunel, Ilker Turkaslan, Philip Torr, Pushmeet Kohli, and Pawan K Mudigonda. A unified view of piecewise linear neural network verification. In *Advances in Neural Information Processing Systems*, pages 4790–4799, 2018.
- [11] Jeremy M Cohen, Elan Rosenfeld, and J Zico Kolter. Certified adversarial robustness via randomized smoothing. *arXiv preprint arXiv:1902.02918*, 2019.
- [12] Gal Dalal, Krishnamurthy Dvijotham, Matej Večerik, Todd Hester, Cosmin Paduraru, and Yuval Tassa. Safe exploration in continuous action spaces. *arXiv preprint arXiv:1801.08757*, 2018.
- [13] John M Danskin. *The theory of max-min with applications*. Siam J. Appl. Math, 1966.
- [14] Alexandre d’Aspremont and Nouredine El Karoui. A stochastic smoothing algorithm for semidefinite programming. *SIAM Journal on Optimization*, 24(3):1138–1177, 2014.
- [15] Lijun Ding, Alp Yurtsever, Volkan Cevher, Joel A Tropp, and Madeleine Udell. An optimal-storage approach to semidefinite programming using approximate complementarity. *arXiv preprint arXiv:1902.03373*, 2019.
- [16] John Duchi, Elad Hazan, and Yoram Singer. Adaptive subgradient methods for online learning and stochastic optimization. *Journal of machine learning research*, 12(Jul):2121–2159, 2011.
- [17] Krishnamurthy Dvijotham, Robert Stanforth, Sven Gowal, Timothy Mann, and Pushmeet Kohli. A dual approach to scalable verification of deep networks. *arXiv preprint arXiv:1803.06567*, 104, 2018.

- [18] Rüdiger Ehlers. Formal verification of piece-wise linear feed-forward neural networks. In Deepak D’Souza and K. Narayan Kumar, editors, *Automated Technology for Verification and Analysis*, pages 269–286, Cham, 2017. Springer International Publishing. ISBN 978-3-319-68167-2.
- [19] Mahyar Fazlyab, Manfred Morari, and George J Pappas. Safety verification and robustness analysis of neural networks via quadratic constraints and semidefinite programming. *arXiv preprint arXiv:1903.01287*, 2019.
- [20] Mahyar Fazlyab, Alexander Robey, Hamed Hassani, Manfred Morari, and George Pappas. Efficient and accurate estimation of lipschitz constants for deep neural networks. In *Advances in Neural Information Processing Systems*, pages 11423–11434, 2019.
- [21] Timon Gehr, Matthew Mirman, Dana Drachler-Cohen, Petar Tsankov, Swarat Chaudhuri, and Martin Vechev. Ai 2: Safety and robustness certification of neural networks with abstract interpretation. In *Security and Privacy (SP), 2018 IEEE Symposium on*, 2018.
- [22] Sven Gowal, Krishnamurthy Dvijotham, Robert Stanforth, Rudy Bunel, Chongli Qin, Jonathan Uesato, Timothy Mann, and Pushmeet Kohli. On the effectiveness of interval bound propagation for training verifiably robust models. *arXiv preprint arXiv:1810.12715*, 2018.
- [23] Sven Gowal, Krishnamurthy Dj Dvijotham, Robert Stanforth, Rudy Bunel, Chongli Qin, Jonathan Uesato, Relja Arandjelovic, Timothy Mann, and Pushmeet Kohli. Scalable verified training for provably robust image classification. In *Proceedings of the IEEE International Conference on Computer Vision*, pages 4842–4851, 2019.
- [24] Sven Gowal, Chongli Qin, Po-Sen Huang, Taylan Cemgil, Krishnamurthy Dvijotham, Timothy Mann, and Pushmeet Kohli. Achieving robustness in the wild via adversarial mixing with disentangled representations. In *Proceedings of the IEEE/CVF Conference on Computer Vision and Pattern Recognition*, pages 1211–1220, 2020.
- [25] Christoph Helmberg and Franz Rendl. A spectral bundle method for semidefinite programming. *SIAM Journal on Optimization*, 10(3):673–696, 2000.
- [26] Guy Katz, Clark Barrett, David L Dill, Kyle Julian, and Mykel J Kochenderfer. Reluplex: An efficient smt solver for verifying deep neural networks. In *International Conference on Computer Aided Verification*, pages 97–117. Springer, 2017.
- [27] Diederik P Kingma and Jimmy Ba. Adam: A method for stochastic optimization. *arXiv preprint arXiv:1412.6980*, 2014.
- [28] Diederik P. Kingma and Max Welling. Auto-encoding variational bayes. In Yoshua Bengio and Yann LeCun, editors, *2nd International Conference on Learning Representations, ICLR 2014, Banff, AB, Canada, April 14-16, 2014, Conference Track Proceedings*, 2014. URL <http://arxiv.org/abs/1312.6114>.
- [29] Torsten Koller, Felix Berkenkamp, Matteo Turchetta, and Andreas Krause. Learning-based model predictive control for safe exploration. In *2018 IEEE Conference on Decision and Control (CDC)*, pages 6059–6066. IEEE, 2018.
- [30] J Zico Kolter and Eric Wong. Provable defenses against adversarial examples via the convex outer adversarial polytope. *arXiv preprint arXiv:1711.00851*, 2017.
- [31] Jacek Kuczynski and Henryk Woźniakowski. Estimating the largest eigenvalue by the power and lanczos algorithms with a random start. *SIAM journal on matrix analysis and applications*, 13(4):1094–1122, 1992.
- [32] Lindsey Kuper, Guy Katz, Justin Gottschlich, Kyle Julian, Clark Barrett, and Mykel Kochenderfer. Toward scalable verification for safety-critical deep networks. *arXiv preprint arXiv:1801.05950*, 2018.
- [33] Guanghui Lan, Zhaosong Lu, and Renato DC Monteiro. Primal-dual first-order methods with $O(1/\epsilon)$ iteration-complexity for cone programming. *Mathematical Programming*, 126(1):1–29, 2011.

- [34] Cornelius Lanczos. *An iteration method for the solution of the eigenvalue problem of linear differential and integral operators*. United States Governm. Press Office Los Angeles, CA, 1950.
- [35] Mathias Lecuyer, Vaggelis Atlidakis, Roxana Geambasu, Daniel Hsu, and Suman Jana. Certified robustness to adversarial examples with differential privacy. *arXiv preprint arXiv:1802.03471*, 2018.
- [36] Claude Lemaréchal and François Oustry. Nonsmooth algorithms to solve semidefinite programs. In *Advances in linear matrix inequality methods in control*, pages 57–77. SIAM, 2000.
- [37] Changliu Liu, Tomer Arnon, Christopher Lazarus, Clark Barrett, and Mykel J Kochenderfer. Algorithms for verifying deep neural networks. *arXiv preprint arXiv:1903.06758*, 2019.
- [38] Aleksander Madry, Aleksandar Makelov, Ludwig Schmidt, Dimitris Tsipras, and Adrian Vladu. Towards deep learning models resistant to adversarial attacks. *arXiv preprint arXiv:1706.06083*, 2017.
- [39] Matthew Mirman, Timon Gehr, and Martin Vechev. Differentiable abstract interpretation for provably robust neural networks. In *International Conference on Machine Learning*, pages 3575–3583, 2018.
- [40] Teodor Mihai Moldovan and Pieter Abbeel. Safe exploration in markov decision processes. *arXiv preprint arXiv:1205.4810*, 2012.
- [41] Renato DC Monteiro. First-and second-order methods for semidefinite programming. *Mathematical Programming*, 97(1-2):209–244, 2003.
- [42] Yurii Nesterov. Smoothing technique and its applications in semidefinite optimization. *Mathematical Programming*, 110(2):245–259, 2007.
- [43] Yurii Nesterov. *Lectures on convex optimization*, volume 137. Springer, 2018.
- [44] T. E. Oliphant. Python for scientific computing. *Computing in Science Engineering*, 9(3):10–20, 2007.
- [45] Neal Parikh and Stephen Boyd. Proximal algorithms. *Foundations and Trends in optimization*, 1(3):127–239, 2014.
- [46] Beresford N Parlett. *The symmetric eigenvalue problem*, volume 20. siam, 1998.
- [47] Adam Paszke, Sam Gross, Francisco Massa, Adam Lerer, James Bradbury, Gregory Chanan, Trevor Killeen, Zeming Lin, Natalia Gimelshein, Luca Antiga, et al. Pytorch: An imperative style, high-performance deep learning library. In *Advances in Neural Information Processing Systems*, pages 8024–8035, 2019.
- [48] Barak A Pearlmutter. Fast exact multiplication by the hessian. *Neural computation*, 6(1): 147–160, 1994.
- [49] Chongli Qin, Krishnamurthy (Dj) Dvijotham, Brendan O’Donoghue, Rudy Bunel, Robert Stanforth, Sven Gowal, Jonathan Uesato, Grzegorz Swirszcz, and Pushmeet Kohli. Verification of non-linear specifications for neural networks. In *International Conference on Learning Representations*, 2019. URL <https://openreview.net/forum?id=HyeFAsRctQ>.
- [50] Haonan Qiu, Chaowei Xiao, Lei Yang, Xinchun Yan, Honglak Lee, and Bo Li. Semanticadv: Generating adversarial examples via attribute-conditional image editing. *arXiv preprint arXiv:1906.07927*, 2019.
- [51] Aditi Raghunathan, Jacob Steinhardt, and Percy Liang. Certified defenses against adversarial examples. In *International Conference on Learning Representations*, 2018. URL <https://openreview.net/forum?id=ByS4ob-Rb>.
- [52] Aditi Raghunathan, Jacob Steinhardt, and Percy S Liang. Semidefinite relaxations for certifying robustness to adversarial examples. In *Advances in Neural Information Processing Systems*, pages 10877–10887, 2018.

- [53] James Renegar. Efficient first-order methods for linear programming and semidefinite programming. *arXiv preprint arXiv:1409.5832*, 2014.
- [54] Hadi Salman, Greg Yang, Huan Zhang, Cho-Jui Hsieh, and Pengchuan Zhang. A convex relaxation barrier to tight robust verification of neural networks. *arXiv preprint arXiv:1902.08722*, 2019.
- [55] Hadi Salman, Greg Yang, Huan Zhang, Cho-Jui Hsieh, and Pengchuan Zhang. A convex relaxation barrier to tight robustness verification of neural networks. *CoRR*, abs/1902.08722, 2019. URL <http://arxiv.org/abs/1902.08722>.
- [56] Gagandeep Singh, Timon Gehr, Matthew Mirman, Markus Püschel, and Martin Vechev. Fast and effective robustness certification. In S. Bengio, H. Wallach, H. Larochelle, K. Grauman, N. Cesa-Bianchi, and R. Garnett, editors, *Advances in Neural Information Processing Systems 31*, pages 10802–10813. Curran Associates, Inc., 2018. URL <http://papers.nips.cc/paper/8278-fast-and-effective-robustness-certification.pdf>.
- [57] Christian Szegedy, Wojciech Zaremba, Ilya Sutskever, Joan Bruna, Dumitru Erhan, Ian Goodfellow, and Rob Fergus. Intriguing properties of neural networks. *arXiv preprint arXiv:1312.6199*, 2013.
- [58] Tijmen Tieleman and Geoffery Hinton. Rmsprop gradient optimization. URL http://www.cs.toronto.edu/tijmen/csc321/slides/lecture_slides_lec6.pdf, 2014.
- [59] Vincent Tjeng, Kai Y. Xiao, and Russ Tedrake. Evaluating robustness of neural networks with mixed integer programming. In *International Conference on Learning Representations*, 2019. URL <https://openreview.net/forum?id=HyGIIdiRqtm>.
- [60] Stephen Tu and Jingyan Wang. Practical first order methods for large scale semidefinite programming. Technical report, Technical report, University of California, Berkeley, 2014.
- [61] Jonathan Uesato, Brendan O’Donoghue, Aaron van den Oord, and Pushmeet Kohli. Adversarial risk and the dangers of evaluating against weak attacks. *arXiv preprint arXiv:1802.05666*, 2018.
- [62] Pauli Virtanen, Ralf Gommers, Travis E. Oliphant, Matt Haberland, Tyler Reddy, David Cournapeau, Evgeni Burovski, Pearu Peterson, Warren Weckesser, Jonathan Bright, Stéfan J. van der Walt, Matthew Brett, Joshua Wilson, K. Jarrod Millman, Nikolay Mayorov, Andrew R. J. Nelson, Eric Jones, Robert Kern, Eric Larson, CJ Carey, İlhan Polat, Yu Feng, Eric W. Moore, Jake VanderPlas, Denis Laxalde, Josef Perktold, Robert Cimrman, Ian Henriksen, E. A. Quintero, Charles R Harris, Anne M. Archibald, Antônio H. Ribeiro, Fabian Pedregosa, Paul van Mulbregt, and SciPy 1.0 Contributors. SciPy 1.0: Fundamental Algorithms for Scientific Computing in Python. *Nature Methods*, 17:261–272, 2020. doi: <https://doi.org/10.1038/s41592-019-0686-2>.
- [63] Zaiwen Wen. *First-order methods for semidefinite programming*. Columbia University, 2009.
- [64] Zaiwen Wen, Donald Goldfarb, and Wotao Yin. Alternating direction augmented lagrangian methods for semidefinite programming. *Mathematical Programming Computation*, 2(3-4): 203–230, 2010.
- [65] Tsui-Wei Weng, Huan Zhang, Hongge Chen, Zhao Song, Cho-Jui Hsieh, Duane Boning, Inderjit S Dhillon, and Luca Daniel. Towards fast computation of certified robustness for relu networks. *arXiv preprint arXiv:1804.09699*, 2018.
- [66] Eric Wong and J Zico Kolter. Learning perturbation sets for robust machine learning. *arXiv preprint arXiv:2007.08450*, 2020.
- [67] Eric Wong, Frank Schmidt, Jan Hendrik Metzen, and J Zico Kolter. Scaling provable adversarial defenses. In *Advances in Neural Information Processing Systems*, pages 8400–8409, 2018.
- [68] Alp Yurtsever, Madeleine Udell, Joel A Tropp, and Volkan Cevher. Sketchy decisions: Convex low-rank matrix optimization with optimal storage. *arXiv preprint arXiv:1702.06838*, 2017.
- [69] Alp Yurtsever, Joel A Tropp, Olivier Fercoq, Madeleine Udell, and Volkan Cevher. Scalable semidefinite programming. *arXiv preprint arXiv:1912.02949*, 2019.
- [70] Huan Zhang, Tsui-Wei Weng, Pin-Yu Chen, Cho-Jui Hsieh, and Luca Daniel. Efficient neural network robustness certification with general activation functions. In *Advances in neural information processing systems*, pages 4939–4948, 2018.

A Omitted proofs

A.1 Adversarial robustness as quadratic specification

Consider certifying robustness: For input $x_0 \in \mathbb{R}^d$ with true label i , the network does not misclassify any adversarial example within ℓ_∞ distance of ϵ from x_0 . This property holds if the score of any incorrect class j is always lower than that of i for all perturbations. Thus $\phi(x) = c^\top x_L$ with $c_j = 1$ and $c_i = -1$. The input constraints are also linear: $-\epsilon \leq x_i - x_{0_i} \leq \epsilon$, for $i = 1, 2, \dots, d$.

A.2 Linear and quadratic constraints for ReLU networks

ReLU as quadratic constraints: For the case of ReLU networks, we can do this exactly, as described in [52]. Consider a single activation $x_{\text{post}} = \max(x_{\text{pre}}, 0)$. This can be equivalently written as $x_{\text{post}} \geq 0, x_{\text{post}} \geq x_{\text{pre}}$, stating that x_{post} is greater than 0 and x_{pre} . Additionally, the quadratic constraint $x_{\text{post}}(x_{\text{post}} - x_{\text{pre}}) = 0$, enforces that x_{post} is atleast one of the two. This can be extended to all units in the network allowing us to replace ReLU constraints with quadratic constraints.

A.3 Formulation of bound constrained dual problem

Proposition 1. The optimal value opt of the quadratic verification problem (1) is bounded above by

$$\text{opt}_{\text{relax}} =: \min_{\lambda \geq 0, \kappa \geq 0} \underbrace{c(\lambda) + \frac{1}{2} \mathbf{1}^\top \left[\kappa - \lambda_{\min}^-(\text{diag}(\kappa) - M(\lambda)) \mathbf{1} \right]}_{f(\lambda, \kappa)}, \quad M(\lambda) = \begin{pmatrix} 0 & g(\lambda)^\top \\ g(\lambda) & H(\lambda) \end{pmatrix}, \quad (8)$$

and $\lambda_{\min}^-(Z)$ is the negative portion of the smallest eigen value of Z , i.e. $[\lambda_{\min}(Z)]^-$ and $\kappa \in \mathbb{R}^{1+N}$.

Proof. We start with the Lagrangian in (4) with rescaled activations such that $\ell = -\mathbf{1}$ and $u = \mathbf{1}$, where ℓ and u are lower and upper bounds on the activations $x \in \mathbb{R}^n$ respectively. This normalization is achieved by using pre-computed bounds via bound propagation, which are used to write the quadratic constraints, as in [52].

$$\text{opt} \leq \min_{\lambda \geq 0} \max_{-1 \leq x \leq 1} \left(c(\lambda) + g(\lambda)^\top x + \frac{1}{2} x^\top H(\lambda) x \right). \quad (9)$$

Define

$$\tilde{X} = \begin{pmatrix} 1 & x^\top \\ x & xx^\top \end{pmatrix}$$

In terms of the above matrix, the above Lagrangian relaxation (9) can be equivalently written as:

$$\text{opt} \leq \min_{\lambda \geq 0} \max_{\text{diag}(\tilde{X}) \leq 1} c(\lambda) + \frac{1}{2} \langle M(\lambda), \tilde{X} \rangle, \quad \text{where} \quad (10)$$

$$M(\lambda) = \begin{pmatrix} 0 & g(\lambda)^\top \\ g(\lambda) & H(\lambda) \end{pmatrix} \quad (11)$$

Note that \tilde{X} is always a PSD matrix with diagonal entries bounded above by 1. This yields the following relaxation of (9)

$$\text{opt} \leq \text{opt}_{\text{sdp}} =: \min_{\lambda \geq 0} \max_{\text{diag}(X) \leq 1, X \geq 0} c(\lambda) + \frac{1}{2} \langle M(\lambda), X \rangle. \quad (12)$$

We introduce a Lagrange multiplier $\frac{1}{2} \kappa \in \mathbb{R}^{n+1}$ for the constraint $\text{diag}(X) \leq 1$ ³. Since opt_{sdp} is convex, by strong duality, we have

$$\text{opt}_{\text{sdp}} = \min_{\lambda, \kappa \geq 0} \max_{X \geq 0} c(\lambda) + \frac{1}{2} \left(\langle M(\lambda), X \rangle + \kappa^\top \mathbf{1} - \langle \text{diag}(\kappa), X \rangle \right), \quad (13)$$

$$= \min_{\lambda, \kappa \geq 0} c(\lambda) + \frac{1}{2} \kappa^\top \mathbf{1} \quad \text{s.t.} \quad \text{diag}(\kappa) - M(\lambda) \geq 0, \quad (14)$$

³The factor of $\frac{1}{2}$ is introduced for convenience

where the last equality follows from the facts that (i) when $\text{diag}(\kappa) - M(\lambda)$ is not PSD, $\langle M(\lambda) - \text{diag}(\kappa), X \rangle$ would be unbounded when maximizing over PSD matrices X and (ii) when $\text{diag}(\kappa) - M(\lambda) \geq 0$, the maximum value of inner maximization over PSD matrices X is 0.

Projecting onto the PSD constraint $\text{diag}(\kappa) - M(\lambda) \geq 0$ directly is still expensive. Instead, we take the following approach. For any non-negative (κ, λ) , we generate a *feasible* $(\hat{\kappa}, \hat{\lambda})$ as follows.

$$\hat{\kappa} = \left[\kappa - \lambda_{\min}^- [\text{diag}(\kappa) - M(\lambda)] \mathbf{1} \right]^+, \quad \hat{\lambda} = \lambda \quad (15)$$

In other words, λ remains unchanged with $\hat{\lambda} = \lambda$. To obtain $\hat{\kappa}$, we first compute the minimum eigenvalue λ_{\min} of the matrix $\text{diag}(\kappa) - M(\lambda)$. If this is positive, (κ, λ) are feasible, and $\hat{\kappa} = \kappa, \hat{\lambda} = \lambda$. However, if this is negative, we then add the negative portion of $\lambda_{\min}^- = [\lambda_{\min}]^-$ to the diagonal matrix to make $\text{diag}(\hat{\kappa}) \geq M(\lambda)$, and subsequently project onto the non-negativity constraint. The subsequent projection never decreases the value of $\hat{\kappa}$ and hence $\text{diag}(\hat{\kappa}) - M(\lambda) \geq 0$.

Plugging $\hat{\kappa}, \hat{\lambda}$ in the objective above, and removing the PSD constraint gives us the following final formulation.

$$\text{opt}_{\text{sdp}} = \text{opt}_{\text{relax}} =: \min_{\lambda, \kappa \geq 0} c(\lambda) + \frac{1}{2} \left[\kappa - \lambda_{\min}^- (\text{diag}(\kappa) - M(\lambda)) \mathbf{1} \right]^{\top} \mathbf{1}. \quad (16)$$

Note that feasible κ, λ remain unchanged and hence the equality. \square

A.4 Relaxation comparison to Raghunathan et al. [52]

Our solver (Algorithm 1) uses the formulation described in (5), replicated above in (16). In this section, we show that the above formulation is equivalent to the SDP formulation in [52] when we use quadratic constraints to replace the ReLU constraints, as done in [52] and presented above in Appendix A.2. We show this by showing equivalence with an intermediate SDP formulation below. From Appendix A.3, the solution to this intermediate fomulation matches that of relaxation we optimize (16).

$$\text{opt}_{\text{sdp}} =: \min_{\lambda \geq 0} \max_{\text{diag}(X) \leq 1, X \geq 0} c(\lambda) + \frac{1}{2} \langle M(\lambda), X \rangle. \quad (17)$$

To mirror the block structure in $M(\lambda)$, we write $X \geq 0$ as follows.

$$X = \begin{pmatrix} X_{11} & X_x^\top \\ X_x & X_{xx} \end{pmatrix}, X_{xx} \geq \frac{1}{X_{11}} X_x X_x^\top, \quad (18)$$

where the last condition follows by Schur complements.

The objective then takes the form $\max_{\text{diag}(X_{xx}) \leq 1, X_{11} \leq 1} g(\lambda)^\top X_x + \frac{1}{2} \langle H(\lambda), X_{xx} \rangle$. Note that the feasible set (over X_{xx}, X_x) for $X_{11} = 1$ contains the feasible sets for any smaller X_{11} , by the Schur complement condition above. Since X_{11} does not appear in the objective, we can set $X_{11} = 1$ to obtain the following equality.

$$\text{opt}_{\text{sdp}} = \min_{\lambda \geq 0} \max_{\text{diag}(X) \leq 1, X_{11} = 1, X \geq 0} c(\lambda) + g(\lambda)^\top X_x + \frac{1}{2} \langle H(\lambda), X_{xx} \rangle, \quad (19)$$

where X_{11} is the first entry, and X_x, X_{xx} are the blocks as described in (18).

Prior SDP. Now we start with the SDP formulation in [52]. Recall that we have a QCQP that represents the original verification problem with quadratic constraints on activations. The relaxation in [52] involves introducing a new matrix variable P as follows.

$$P = \begin{pmatrix} P[1] & P[x] \\ P[x] & P[xx] \end{pmatrix} \quad (20)$$

The quadratic constraints are now written in terms of P where $P[x]$ replaces the linear terms and $P[xx]$ replaces the quadratic terms. Raghunathan et al. [52] optimize this primal SDP formulation to obtain $\text{opt}_{\text{prior-sdp}}$. By strong duality, $\text{opt}_{\text{prior-sdp}}$ matches the optimum of the dual problem obtained

via the Lagrangian relaxation of the SDP. In terms of the quantities g, H that we defined in this work ((3) and (4)), we have

$$\text{opt}_{\text{prior-sdp}} = \min_{\lambda \geq 0} \max_{\text{diag}(P) \leq 1, P[1]=1, P \geq 0} \mathcal{L}_{\text{prior-sdp}}(P, \lambda) \quad (21)$$

$$= \min_{\lambda \geq 0} \max_{\text{diag}(P) \leq 1, P[1]=1, P \geq 0} c(\lambda) + g(\lambda)^\top P[x] + \frac{1}{2} \langle H(\lambda), P[xx] \rangle. \quad (22)$$

By redefining matrix P as X , from (19) and (21), we have $\text{opt}_{\text{sdp}} = \text{opt}_{\text{prior-sdp}}$. From (16), we have $\text{opt}_{\text{sdp}} = \text{opt}_{\text{relax}}$ and hence proved that the optimal solution of our formulation matches that of prior work [52] when using the same quadratic constraints as used in [52]. In other words, our reformulation that allows for a subgradient based memory efficient solver does *not* introduce additional looseness over the original formulation that uses a memory inefficient interior point solver.

A.5 Regularization of κ via alternate dual formulation

In Section 5.3, we describe that it can be helpful to regularize $\kappa_{1:n}$ towards 0. This is motivated by the following proposition:

Proposition 3. The optimal value opt is upper-bounded by the alternate dual problem

$$\text{opt} \leq \min_{\lambda, \kappa \geq 0} \underbrace{c(\lambda) + \frac{1}{2} \kappa_0}_{\hat{f}(\lambda, \kappa_0)} \text{ s.t. } \begin{pmatrix} \kappa_0 & -g(\lambda)^\top \\ -g(\lambda) & -H(\lambda) \end{pmatrix} \geq 0 \quad (23)$$

Further, for any feasible solution λ, κ_0 for this dual problem, we can obtain a corresponding solution to $\text{opt}_{\text{relax}}$ with $\lambda, \kappa_0, \kappa_{1:n} = 0, \kappa = (\kappa_0; \kappa_{1:n})$, such that $f(\lambda, \kappa) = \hat{f}(\lambda, \kappa_0)$.

Proof. We begin with the Lagrangian dual

$$\text{opt} \leq \text{opt}_{\text{lagAlt}} =: \min_{\lambda \geq 0} \max_x c(\lambda) + x^\top g(\lambda) + \frac{1}{2} x^\top H(\lambda) x. \quad (24)$$

Note that this is exactly the dual from Equation (4), without the bound constraints on x in the inner maximization. In other words, whereas Equation (4) encodes the bound constraints into both the Lagrangian and the inner maximization constraints, in Equation 24, the bound constraints are encoded in the Lagrangian only.

The inner maximization can be solved in closed form, and is maximized for $x = -H(\lambda)^{-1}g(\lambda)$, yielding

$$\text{opt}_{\text{lagAlt}} = \min_{\lambda \geq 0} c(\lambda) - \frac{1}{2} g(\lambda)^\top H(\lambda) g(\lambda). \quad (25)$$

We can then reformulate using Schur complements:

$$\text{opt}_{\text{lagAlt}} = \min_{\lambda \geq 0, \kappa_0} c(\lambda) + \frac{1}{2} \kappa_0 \text{ s.t. } \kappa_0 \geq -g(\lambda) H(\lambda)^{-1} g(\lambda) \quad (26a)$$

$$= \min_{\lambda \geq 0, \kappa_0} c(\lambda) + \frac{1}{2} \kappa_0 \text{ s.t. } \hat{M}(\lambda) \geq 0 \text{ where} \quad (26b)$$

$$\hat{M}(\lambda) = \begin{pmatrix} \kappa_0 & -g(\lambda)^\top \\ -g(\lambda) & -H(\lambda) \end{pmatrix}. \quad (26c)$$

To see that this provides a corresponding solution to $\text{opt}_{\text{relax}}$, we note that when $\hat{M} \geq 0$, the choice $\kappa = (\kappa_0; \kappa_{1:n}), \kappa_{1:n} = 0$ makes $\text{diag}(\kappa) - M(\lambda) = \hat{M}(\lambda)$, and so $\lambda_{\min}^-[\text{diag}(\kappa) - M(\lambda)] = 0$. Thus, for any solution λ, κ_0 , we have $f(\lambda, \kappa) = \hat{f}(\lambda, \kappa_0) = c(\lambda) + \frac{1}{2} \kappa_0$. □

Remark. Proposition 3 indicates that regularizing $\kappa_{1:n}$ towards 0 corresponds to solving the alternate dual formulation $\text{opt}_{\text{dualAlt}}$, which does not use bound constraints for the inner maximization. In this case, the role of $\kappa_{1:n}$ and $\hat{\kappa}$ is slightly different: even in the case when $\kappa_{1:n}$ is clamped to 0, the bound-constrained formulation allows an efficient projection operator, which in turn provide efficient any-time bounds.

A.6 Informal comparison to standard maximum eigenvalue formulation

Our derivation for Proposition 1 is similar to maximum eigenvalue formulations for dual SDPs – our main emphasis is that when applied to neural networks, we can use autodiff and implicit matrix-vector products to efficiently compute subgradients.

We also mention here a minor difference in derivations for convenience of readers. The common derivation for these maximum eigenvalue formulations starts with an SDP primal under the assumption that all feasible solutions for the matrix variable X have fixed trace. This trace assumption plays an analogous role to our interval constraints in the QCQP (12). These interval constraints also imply a trace constraint (since $\text{diag}(X) \leq 1$ implies $\text{tr}(X) \leq N + 1$), but the interval constraints also allow us to use κ to smooth the optimization. Without κ , any positive eigenvalues of $M(\lambda)$ cause large spikes in the objective – simplifying the objective $f(\lambda, \kappa)$ in (5) reveals the term $(N + 1)\lambda_{\max}^+(M(\lambda))$ which grows linearly with N . As expected, this term also appears in these other formulations [25, 42].

A.7 Proof of Proposition 2

Proposition 2. For any choice of λ satisfying $H(\lambda) = 0$, the optimal choice $\kappa_{\text{opt}}(\lambda)$ is given by

$$\kappa_0^* = \sum_{i=1}^n |g(\lambda)|_i \quad ; \quad \kappa_{1:n}^* = |g(\lambda)|$$

where we have divided $\kappa = [\kappa_0; \kappa_{1:n}]$ into a leading scalar κ_0 and a vector $\kappa_{1:n}$.

Proof. We use the dual expression from Equation (14):

$$\text{opt}_{\text{sdp}} = \min_{\lambda, \kappa \geq 0} c(\lambda) + \frac{1}{2} \kappa^\top \mathbf{1} \quad \text{s.t.} \quad \text{diag}(\kappa) - M(\lambda) \geq 0.$$

Notice that by splitting κ into its leading component κ_0 (a scalar) and the subvector $\kappa_{1:n} = [\kappa_1, \dots, \kappa_n]$ (a vector of the same dimension as x), the constraint between κ, λ evaluates to

$$\text{diag}(\kappa) - M(\lambda) = \begin{pmatrix} \kappa_0 & g(\lambda)^\top \\ g(\lambda) & \text{diag}(\kappa_{1:n}) \end{pmatrix} \geq 0$$

Using Schur complements, we can rewrite the PSD constraint as

$$\left(\text{diag}(\kappa) - M(\lambda) \right) \geq 0 \Leftrightarrow \kappa_0 \geq \sum_{i \geq 1} \kappa_i^{-1} (g(\lambda))_i^2$$

Since the objective is monotonically increasing in κ_0 , the optimal choice for κ_0 is the lower bound above $\kappa_0 \geq \sum_{i \geq 1} \kappa_i^{-1} (g(\lambda))_i^2$. Given this choice, the objective in terms of $\kappa_{1:n}$ becomes

$$\sum_{i \geq 1} \kappa_i + \frac{(g(\lambda))_i^2}{\kappa_i}$$

By the AM-GM inequality, the optimal choice for the remaining terms $\kappa_{1:n}$ is then $\kappa_{1:n} = |g(\lambda)|$. \square

B Experimental details

B.1 Verifying Adversarial Robustness: Training and Hyperparameter Details

Optimization details. We perform subgradient descent using the Adam [27] update rule for MLP experiments, and RMSProp for CNN experiments. We use an initial learning rate of $1e - 3$, which we anneal twice by 10. We use 15K optimization steps for all MLP experiments, 60K for CNN experiments on MNIST, and 150K on CIFAR-10. All experiments run on a single P100 GPU.

Adaptive learning rates For MLP experiments, we use an adaptive learning rate for dual variables associated with the constraint $x_{i+1} \odot (x_{i+1} - \mathbb{I}_i(x_i)) \leq 0$, as mentioned in Section 5.3. In early experiments for MLP-Adv, we observed very sharp curvature in the dual objective with respect to these variables – the gradient has values on the order $\approx 1e3$ while the solution at convergence has values on the order of $\approx 1e-2$. Thus, for all MLP experiments, we decrease learning rates associated with these variables by a $10\times$ factor. While SDP-FO produced meaningful bounds even without this adjustment, we observed that this makes optimization significantly more stable for MLP experiments. This adjustment was not necessary for CNN experiments.

Training Modes We conduct experiments on networks trained in three different modes. **Nor** indicates the network was trained only on unperturbed examples, with the standard cross-entropy loss. **Adv** networks use adversarial training [38]. **Mix** networks average the adversarial and normal losses, with equal weights on each. We find that **Mix** training, while providing a significant improvement in test-accuracy, renders the model less verifiable (across verification methods) than training only with adversarial examples.

The suffix **-4** in the network name (e.g. CNN-A-Mix-4) indicates networks trained with the large perturbation radius $\epsilon_{\text{train}} = 4.4/255$. We find that using larger ϵ_{train} implicitly facilitates verification at smaller ϵ (across verification methods), but is accompanied by a significant drop in clean accuracy. For all other networks, we choose ϵ_{train} to match the evaluation ϵ : i.e. generally $\epsilon = 0.1$ on MNIST and $\epsilon = 2.2/255$ on CIFAR-10 (which slightly improves adversarial robustness relative to $\epsilon = 2/255$ as reported in [22]).

Pre-trained networks For the networks **MLP-LP**, **MLP-SDP**, **MLP-Adv**, we use the trained parameters from [52], and for the networks **MLP-Nor**, **MLP-Adv-B** we use the trained parameters from [55].

Model Architectures Each model architecture is associated with a prefix for the network name. Table 2 summarizes the CNN model architectures. The MLP models are taken directly from [52, 55] and use fully-connected layers with ReLU activations. The number of neurons per layer is as follows: **MLP-Adv** 784-200-100-50-10, **MLP-LP/MLP-SDP** 784-500-10, **MLP-B/MLP-Nor** 784-100-100-10.

Model	CNN-A	CNN-B
Architecture	CONV 16 4×4+2	CONV 32 5×5+2
	CONV 32 4×4+1	CONV 128 4×4+2
	FC 100	FC 250
	FC 10	FC 10

Table 2: Architecture of CNN models used on MNIST and CIFAR-10. Each layer (except the last fully connected layer) is followed by ReLU activations. CONV $T \times W \times H + S$ corresponds to a convolutional layer with T filters of size $W \times H$ with stride of S in both dimensions. FC T corresponds to a fully connected layer with T output neurons.

B.2 Verifying VAEs

Architecture Details We train a VAE on the MNIST dataset with the architecture detailed in Table 3.

Encoder	Decoder
FC 512	FC 1568
FC 512	CONV-T 32 3×3+2
FC 512	CONV-T 3×3+1
FC 16	

Table 3: The VAE consists of an encoder and a decoder, and the architecture details for both the encoder and the decoder are provided here. CONV-T $T \times W \times H + S$ corresponds to a transpose convolutional layer with T filters of size $W \times H$ with stride of S in both dimensions.

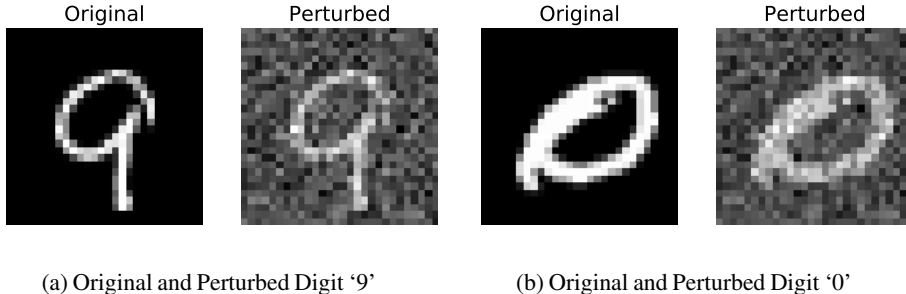


Figure 3: Two digits from the MNIST data set, and the corresponding images when perturbed with Gaussian noise, whose squared ℓ_2 -norm is equal to the threshold ($\tau = 40.97$). τ corresponds to threshold on the reconstruction error used in equation (7).

Optimization details. We perform subgradient descent using RMSProp with an initial learning rate of $1e-3$, which we anneal twice by 10. All experiments run on a single P100 GPU, and each verification instance takes under 7 hours to run.

Computing bounds on the reconstruction loss based on interval bound propagation Interval bound propagation lets us compute bounds on the activations of the decoder, given bounded l_∞ perturbations in the latent space of the VAE. Given a lower bound lb and an upper bound ub on the output of the decoder, we can compute an upper bound on the reconstruction error $\|s - \hat{s}\|_2$ over all valid latent perturbations as $\|\max\{|ub - s|, |s - lb|\}\|_2^2$, where \max represents the element-wise maximum between the two vectors. We visualize images perturbed by noise corresponding to the threshold τ on the reconstruction error in Section 6.2 in Figure 3.

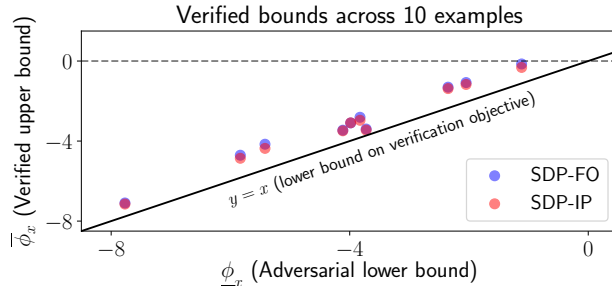
C Additional results

C.1 Detailed comparison to off-the-shelf solver

Setup We isolate the impact of optimization by comparing performance to an off-the-shelf solver with the same SDP relaxation. For this experiment, we use the MLP-Adv network from [51], selecting quadratic constraints to attain an equivalent relaxation to [51]. We compare across 10 random examples, using the target label with the highest loss under a PGD attack, i.e. the target label closest to being misclassified. For each example, we measure $\underline{\Phi}_{\text{PGD}}$, $\overline{\Phi}_{\text{SDP-IP}}$, and $\overline{\Phi}_{\text{SDP-FO}}$, where $\overline{\Phi}$ and $\underline{\Phi}$ are as defined in Section 6.1. Since the interior point method used by MOSEK can solve SDPs exactly for small-scale problems, this allows analyzing looseness incurred due to the relaxation vs. optimization. In particular, $\overline{\Phi}_{\text{SDP-IP}} - \underline{\Phi}_{\text{PGD}}$ is the relaxation gap, plus any suboptimality for PGD, while $\overline{\Phi}_{\text{SDP-IP}} - \overline{\Phi}_{\text{SDP-FO}}$ is the optimization gap due to inexactness in the SDP-FO dual solution.

Results We observe that SDP-FO converges to a near-optimal dual solution in all 10 examples. This is shown in Figure 4. Quantitatively, the relaxation gap $\overline{\Phi}_{\text{SDP-IP}} - \underline{\Phi}_{\text{PGD}}$ has a mean of 0.80 (standard deviation 0.22) over the 10 examples, while the optimization gap $\overline{\Phi}_{\text{SDP-IP}} - \overline{\Phi}_{\text{SDP-FO}}$ has a mean of 0.10 (standard deviation 0.07), roughly $8\times$ smaller. Thus, SDP-FO presents a significantly more scalable approach, while sacrificing little in precision for this network.

Remark. While small-scale problems can be solved exactly with second-order interior point methods, these approaches have poor asymptotic scaling factors. In particular, both the SDP primal and dual problems involve matrix variables with number of elements quadratic in the number of network activations N . Solving for the KKT stationarity conditions (e.g. via computing the Cholesky decomposition) then requires memory $O(N^4)$. At a high-level, SDP-FO uses a first-order method to save a quadratic factor, and saves another quadratic factor through use of iterative algorithms to avoid materializing the $M(\lambda)$ matrix. SDP-FO achieves $O(Nk)$ memory usage, where k is the number of Lanczos iterations, and in our experiments, we have found $k \ll N$ suffices for Lanczos convergence.



(a) MNIST, MLP-Adv

Figure 4: *Comparison to off-the-shelf solver.* For 10 examples on MNIST, we plot the verified upper bound on ϕ_x against the adversarial lower bound (using a single target label for each), comparing SDP-FO to the optimal SDP bound found with SDP-IP (using MOSEK). In all cases, the SDP-FO bound is very close to the SDP-IP bound, demonstrating that SDP-FO converges to a near-optimal dual solution. Note that in many cases, the scatter points for SDP-FO and SDP-IP are directly overlapping due to the small gap.

C.2 Investigation of relaxation tightness for MLP-Adv

Setup The discussion above in Appendix C.1 suggests that SDP-FO is a sufficiently reliable optimizer so that the main remaining obstacle to tight verification is tight relaxations. In our main experiments, we use simple interval arithmetic [39, 23] for bound propagation, to match the relaxation in [51]. However, by using CROWN [70] for bound propagation, we can achieve a tighter relaxation.

Results Using CROWN bounds in place of interval arithmetic bounds improves the overall verified accuracy from 83.0% to 91.2%. This closes most of the gap to the PGD upper bound of 93.4%. For this model, while the SDP relaxation still yields meaningful bounds when provided very loose initial bounds, the SDP relaxation still benefits significantly from tighter initial bounds. More broadly, this suggests that SDP-FO provides a reliable optimizer, which combines naturally with development of tighter SDP relaxations.

C.3 Verifying Adversarial Robustness: Additional Results

Table 4 provides additional results on verifying adversarial robustness for different perturbation radii and training modes. Here, we consider perturbations and training-modes not included in Table 1. We find that across settings, **SDP-FO** outperforms the **LP**-relaxation.

Dataset	Epsilon	Model	Training Epsilon	Accuracy		Verified Accuracy	
				Nominal	PGD	SDP-FO (Ours)	LP
MNIST	$\epsilon = 0.3$	CNN-A-Adv	$\epsilon_{\text{train}} = 0.3$	98.6%	80.0%	43.4%	0.2%
CIFAR-10	$\epsilon = \frac{2}{255}$	CNN-A-Adv	$\epsilon_{\text{train}} = \frac{2.2}{255}$	68.7%	53.8%	39.6%	5.8%
		CNN-A-Adv-4	$\epsilon_{\text{train}} = \frac{4.4}{255}$	56.4%	49.4%	40.0%	38.9%
	$\epsilon = \frac{8}{255}$	CNN-A-Adv	$\epsilon_{\text{train}} = \frac{8.8}{255}$	46.9%	30.6%	18.0%	3.8%
		CNN-A-Mix	$\epsilon_{\text{train}} = \frac{8.8}{255}$	56.7%	26.4%	9.0%	0.1%

Table 4: Comparison of verified accuracy across various networks and perturbation radii. All SDP-FO numbers computed on the first 100 test set examples, and numbers for **LP** on the first 1000 test set examples. The perturbations and training-modes considered here differ from those in Table 1. For all networks, SDP-FO outperforms the **LP**-relaxation baseline.

C.4 Comparison between Lanczos and exact eigendecomposition

All final numbers we report use the minimum eigenvalue from an exact eigendecomposition (we use the `eigh` routine available in SciPy [62]). However, the exact decomposition is far too expensive to

use during optimization. On all networks we studied, Lanczos provides a reliable surrogate, while using dramatically less computation. For example, for CNN-A-Mix, the average gap between the exact and Lanczos dual bounds – the values of Equation (5) using the true λ_{\min} compared to the Lanczos approximation of λ_{\min}) – is 0.14 with standard deviation 0.07. This gap is small compared to the overall gap between the verified upper and adversarial lower bounds, which has mean 0.60 with standard deviation 0.22. We observed similarly reliable Lanczos performance across models, for both image classifier and VAE models in Sections 6.1 and 6.2.

At the same time, Lanczos is dramatically faster than the exact eigendecomposition: roughly 0.1 seconds (using 200 Lanczos iterations) compared to 5 minutes. For the VAE model, this gap is even larger: roughly 0.2 seconds compared to 2 hours. For even larger models, it may be infeasible to compute the exact eigendecomposition even once. Although unnecessary in our current work, high-confidence approximation bounds for eigenvectors and associated eigenvalues from Lanczos can be applied in such cases [31, 46].